Resonance in the collision of two discrete intrinsic localized excitations

David Cai, A. R. Bishop, and Niels Grønbech-Jensen
Theoretical Division and Center for Nonlinear Studies, Los Alamos National Laboratory, Los Alamos, New Mexico 87545
(Received 10 June 1997)

The collision dynamics of two solitonlike localized excitations in a nonintegrable discrete $(1+1)$-dimensional nonlinear Schrödinger system is studied numerically. It is demonstrated that the collision dynamics exhibits a complicated resonance structure of interlacing bound-state regions and escape regions of localized excitations with a sensitive dependence on the incoming energies of the localized excitations. We emphasize that this resonance is a combined effect of discreteness and nonintegrability of the system and contrast it with topological kink-antikink collisions in ϕ^4 and related systems. [S1063-651X(97)06811-6]

PACS number(s): 42.65.Tg, 63.20.Pw, 46.10.+z, 42.81.Dp

Intrinsic localized excitations are a longstanding and important topic in the context of intrinsic collapse to self-localized states in nonlinear systems, which has wide physical significance in plasmas, fluids, optics, solid-state, and biomolecular modeling [1,2]. Pure $(1+1)$-dimensional integrable systems provide rigorous examples of self-localized states in the form of solitons and are by now well understood [3,4]. In particular, the interaction of these solitons can be simply described as pure elastic collisions with ''space'' shifts. The interaction dynamics is simple in the sense that solitons do not interact in the nonlinear spectral space from the inverse scattering transform (IST) viewpoint. In a realistic physical setting, complete integrability is often destroyed by physical ''perturbations'' such as integrability-breaking terms in partial differential equations, dimensionality, lattice discreteness, disorder, and fluctuations (quantum and thermal) [1,2,5]. As a consequence, mechanisms controlling the collapse to stable localized excitations become physically more complicated and are mathematically less well understood. Recently, *discrete* intrinsic localized excitations have been increasingly studied, as they appear to be generally robust objects and their existence does not require mathematically stringent integrability [6]. The existence and stability of these excitations are consequences of the combined effect of discreteness and nonlinearity of the system [6–9]. Some rigorous mathematical results regarding their existence and stability have been obtained via, e.g., the application of implicit function theorems [10–12]. Many aspects of the intrinsic localized states have been studied by the rotating-wave approximation [8,13] or numerically more exact methods such as the Newton iteration method [14–16]. Full dynamical simulations have also been performed to illustrate dynamical properties of these excitations (see, e.g., [17–27]). However, most of these studies have concentrated mainly on single discrete localized excitations. The question of how these excitations interact is yet to receive much attention [28]. Obviously, addressing this issue is a natural and important step in extending our understanding of the dynamics of discrete localized excitations in spite of analytical and numerical difficulties involved in this pursuit.

In the present work, we undertake a detailed numerical study of the collision of two localized excitations in a discrete nonlinear Schrödinger (DNLS) system, which is a continuously tunable, generally nonintegrable system, with the completely integrable Ablowitz-Ladik equation as one limit [9,29]. For this system, the existence, stability, and various other aspects of a single solitonlike localized excitation have been clarified using perturbation theories based on, e.g., the inverse scattering transform and Melnikov analysis [9,30–33]. As these works have demonstrated, this system encapsulates many important issues involved in studies of intrinsic localized excitations in a theoretical framework of conceptual simplicity and analytical tractability. We emphasize that this DNLS system has very rich dynamics, which the system in its integrable limit does not possess either in the discrete form or in the continuous limit. On the basis of a careful numerical study, we will demonstrate below that the interaction of two localized excitations has a complicated resonance structure. Namely, the collision process exhibits a series of resonant trapping (bound states) and escaping (transmission) of the localized excitations with a sensitive dependence on their incoming energies. This should be contrasted with the two integrable cases. On the one hand, the interaction of two solitons in the Ablowitz-Ladik system is elastic due to integrability, therefore lending such a resonance structure impossible. On the other hand, the interaction of two solitons in the continuous limit, in which our system becomes the completely integrable nonlinear Schrödinger equation, has again simple elastic dynamics without any resonance. Thus this resonance structure is a combined effect of discreteness and nonintegrability. In the following, we will first briefly review the dynamics of a single localized excitation to set the stage for our main work, i.e., the collision dynamics of two such structures. Then we will present detailed results of the resonance structure in this system.

The one-dimensional DNLS equation we study is [9]

$$i\dot{\psi}_n = -(\psi_{n+1}+\psi_{n-1}) - [\mu(\psi_{n+1}+\psi_{n-1}) + 2\nu\psi_n]|\psi_n|^2, \tag{1}$$

where the overdot stands for the derivative with respect to time t, n is a site index, and $\mu \geqslant 0$. This system possesses the Hamiltonian

$$\mathcal{H}=-\sum_n\ (\psi_n\psi_{n+1}^*+\psi_n^*\psi_{n+1})-\frac{2\nu}{\mu}\sum_n\ |\psi_n|^2$$

$$+\frac{2\nu}{\mu^2}\sum_n\ \ln(1+\mu|\psi_n|^2) \tag{2}$$

with the deformed Poisson brackets

$$\{\psi_n,\psi_m^*\}=i(1+\mu|\psi_n|^2)\,\delta_{nm}, \tag{3}$$

$$\{\psi_n,\psi_m\}=\{\psi_n^*,\psi_m^*\}=0. \tag{4}$$

In general, dynamical variables B and C obey

$$\{B,C\}=i\sum_n\ \left(\frac{\partial B}{\partial\psi_n}\frac{\partial C}{\partial\psi_n^*}-\frac{\partial B}{\partial\psi_n^*}\frac{\partial C}{\partial\psi_n}\right)(1+\mu|\psi_n|^2). \tag{5}$$

Equation (1) is the equation of motion

$$\dot{\psi}_n=\{\mathcal{H},\psi_n\}. \tag{6}$$

In addition to the conserved energy $\mathcal{H}$, the quantity

$$\mathcal{N}=\frac{1}{\mu}\sum_n\ \ln(1+\mu|\psi_n|^2) \tag{7}$$

is also conserved and serves as a norm. These conserved quantities were frequently monitored in our numerical simulations to ensure accuracy of the numerical schemes. In the integrable Ablowitz-Ladik limit, a single localized excitation is an Ablowitz-Ladik soliton [9]

$$\psi_n=\sinh\,\beta\ \mathrm{sech}[\beta(n-x)]e^{i\alpha(n-x)+i\sigma}, \tag{8}$$

the parameters of which obey

$$\dot{\beta}=0, \tag{9}$$

$$\dot{\alpha}=0, \tag{10}$$

$$\dot{x}=\frac{2\sinh\beta}{\beta}\sin\,\alpha, \tag{11}$$

$$\dot{\sigma}=2\cos\alpha\,\cosh\beta+2\alpha\,\sin\alpha\frac{\sinh\beta}{\beta}. \tag{12}$$

In the perturbed case, to the first order in ν in the adiabatic approximation, an IST-based perturbation theory leads to a localized excitation with the same functional form as Eq. (8) and perturbed dynamics for the parameters. We will use this functional form (8) as the initial condition for the localized excitations in our numerical simulations (see below). The dynamics of the parameters now become [34] (for details, see [30])

$$\dot{\beta}=0, \tag{13}$$

$$\dot{\alpha}=-\frac{\partial}{\partial x}\mathcal{H}_{\mathrm{eff}}, \tag{14}$$

$$\dot{x}=\frac{\partial}{\partial\alpha}\mathcal{H}_{\mathrm{eff}} \tag{15}$$

with

$$\mathcal{H}_{\mathrm{eff}}=\mathcal{K}+\mathcal{V}, \tag{16}$$

$$\mathcal{K}=-\frac{2\sinh\beta}{\beta}\sin\alpha, \tag{17}$$

$$\mathcal{V}=-\nu\sum_{s=1}^{\infty}\ \frac{4\pi^2 s\,\sinh^2\beta}{\beta^3\,\sinh(\pi^2 s/\beta)}\cos(2\pi s x). \tag{18}$$

This gives rise to the following picture for the motion of a single localized structure: It can be regarded as a point particle described by the general coordinates (x,α) in an effective periodic potential, i.e., a Peierls-Nabarro barrier.

Next we turn to the demonstration of the richness of the system (1) through the interaction dynamics of *two* localized excitations using full numerical simulations of the system (1). As noted above, for $\nu=0$, the integrable limit of Eq. (1), two solitons will simply collide elastically, passing through each other with the same asymptotic velocity, before and after collision, at large separations. The collision is signified only by a ''space shift'' in the collision region. Likewise, on approaching the continuum limit, the nonintegrability becomes weaker and weaker and we again have an integrable soliton collision case in the continuum limit. Due to nonintegrability and discreteness, it turns out that collisions of two localized excitations with $\nu\neq 0$ have a very complicated dynamics and manifest intriguing resonance structures. As we can see below, some subtleties in the collisions indicate a different mechanism from that which has been learned in the collision dynamics of a topological kink and an antikink in the continuous ϕ^4 system, modified double sine-Gordon systems, or related kink interactions with a point impurity [35–39].

First we discuss the collision of two localized excitations with equal amplitudes. The numerical simulation of this dynamics in system (1) is implemented as follows. The lattice of the system is indexed from $n=0$ to $n=N-1$. The boundary conditions are reflecting, i.e.,

$$\psi_{-1}=\psi_1,\quad \psi_{N-2}=\psi_N. \tag{19}$$

With these boundary conditions, in the region $n<0$, we create a mirror image of the system of $n>0$. As justified above by perturbation theory, we use the functional form (8) as our initial localized state situated at x_0, which is chosen sufficiently far from $n=0$ that we can view the initial condition for the system as two widely separated localized excitations (one is the mirror image in the $n<0$ region) with exponentially small overlap around $n=0$. Since we set the collision region near $n=0$, the other end of the system has basically vanishing ψ_n. For $t>0$, this localized excitation travels towards $n=0$ and collides with its mirror image. We chose a sufficiently large N to avoid boundary effects, such as reflected radiations from the $N-1$ end. In our simulations, typically, $N=500$ was used with the choice of $\beta\sim 1$ for the localized excitation (8). This size is sufficiently large to minimize boundary effects in the collision region near $n=0$ while it is not too large to exact our computing resources.

Now we describe the resonance phenomenon in the case of varying α. In simulations, the nonintegrable parameter ν

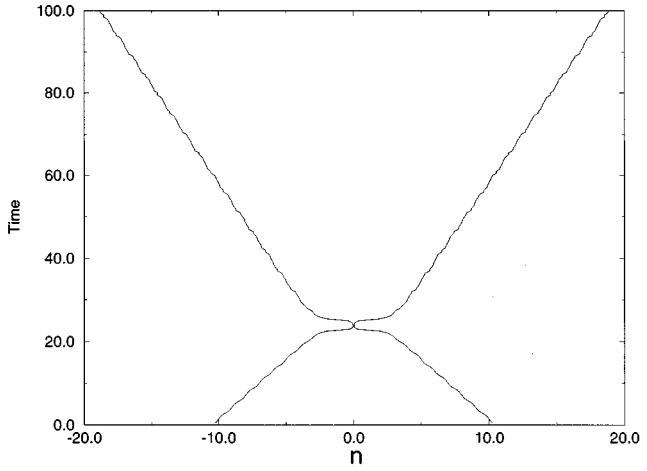

FIG. 1. Trajectory of two colliding localized excitations. After collision, these two excitations separate. Here $|\alpha|=0.15$, $\beta=1$, $x_0=10.5$, $\mu=1$, and $\nu=-0.1$ in system (1).

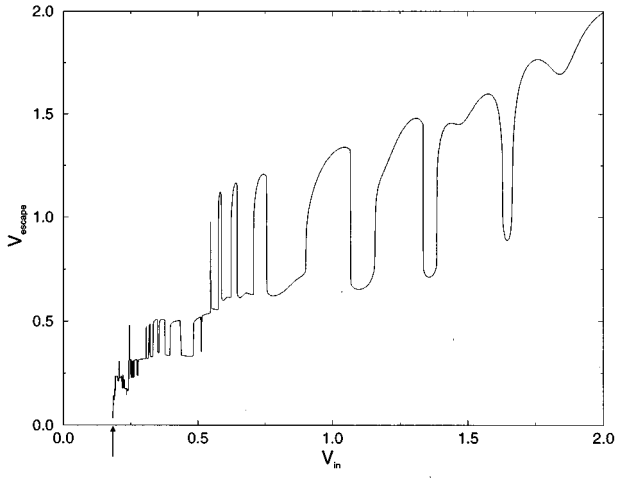

FIG. 2. Escape velocity of a localized excitation after colliding with its mirror image as a function of the incoming velocity ($\mu=1$ and $\nu=-0.1$). The parameters for the initial profile (8) are $\beta=1$ and $x_0=10.5$. The data of the incoming velocity in the region below the arrow are not shown.

should not be too large; otherwise a localized state initialized with the soliton form (8) will change its shape greatly by emitting strong radiation and the evolution of this localized state will have severe radiative effects. Thus $\nu=-0.1$ was used. As can be expected, for $\alpha \ll \pi$, the incoming velocity of the localized excitation is a monotonically increasing function of $|\alpha|$. This was indeed confirmed in our numerical simulations. We controlled the initial velocity of a localized excitation by controlling the value of the parameter α. For large incoming velocities, we observed that, after a localized excitation collides with its mirror image, they separate. They do not return to execute a second collision. A typical trajectory of this case is shown in Fig. 1. The trajectory shown is the temporal trace of the position of the maximum density of $|\psi_n|$. The interpolated maximum point at time t is obtained via the parabolic Simpson interpolation algorithm, using the first three largest amplitudes out of the set of $\{|\psi_n(t)|$, all $n\}$ and treating n as if it were a continuous variable, whence the position of the interpolated maximum is a continuous variable. Note that we only simulated the system (1) for $n \geqslant 0$ and that the $n<0$ portion of Fig. 1 is merely a mirror reflection of the right-hand side of the figure, plotted graphically to give a sense of symmetry. This graphical convention will be used for all the remaining trajectory plots. For an incoming velocity greater than the critical value, $V_{\text{in},c}=0.1837$, only this type of separating state is observed. The measured escape velocity as a function of the incoming velocity displays rather complicated structures as shown in Fig. 2. We note that it has a somewhat ''self-similar'' repeating pattern, while shrinking towards the small velocity regime, although the pattern is not very regular. A blowup of the incoming velocity region indicated by the arrow in Fig. 2 is shown in Fig. 3. Clearly, the self-similar pattern persists. This complicated dependence of the escape velocity on the incoming velocity is a first glimpse of the complexity of the collision dynamics. Before turning to even more unusual phenomena, we comment that, in general, it is difficult to define an instantaneous velocity on a lattice. Thus the concept of velocity in a lattice system is inherently in an average sense. Only in rare situations in which a solution possesses the continuous translational symmetry are we able to use the concept of the instantaneous velocity, such as in the case of the soliton solutions for the Ablowitz-Ladik equation. Bearing this in mind, we obtained the incoming velocity of a localized excitation by measuring the time elapsed between the time for the localized excitation peak to arrive at a site $n=n_0$ and the time at the site $n=n_0-4$, where $n_0=10$ was used in our measurements. Similarly, the escape velocity is computed by $V_{\text{escape}}=4/\delta t$, where δt is the time interval between the instant when the localized excitation peak arrives at the site n_0-4 and the instant when it arrives at n_0.

One would expect that there are two different types of states formed after collision, i.e., one being the escaping states described above and the other being bound states when the two localized excitations become trapped. The bound states can be anticipated based on the following argument. In the very small incoming velocity regime, localized excita-

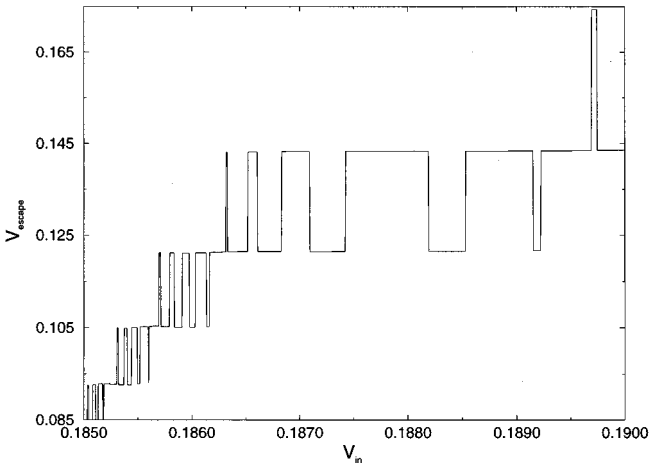

FIG. 3. Escape velocity of a localized excitation after colliding with its mirror image as a function of the incoming velocity with the initial profile (8) with $\beta=1$ and $x_0=10.5$. This is a blowup of Fig. 2 in the region indicated by the arrow in Fig. 2. $\mu=1$ and $\nu=-0.1$ in system (1).

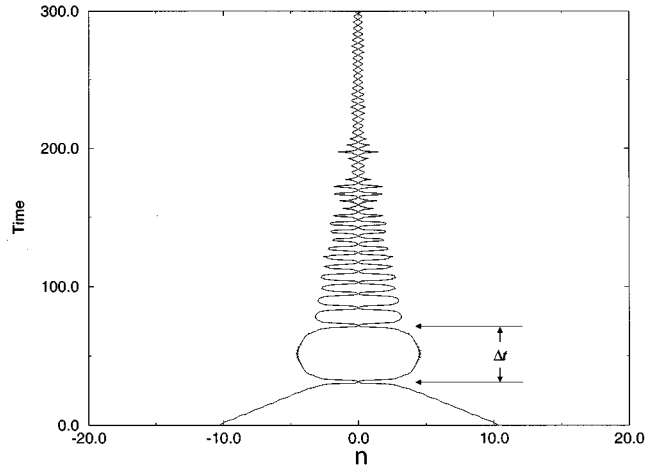

FIG. 4. Upon collision, two localized excitations form a long-lived breathing bound state. The parameters for the initial condition (8) are $|\alpha|=0.11$ and $\beta=1$. The system parameters are $\mu=1$ and $\nu=-0.1$. Δt is the time between the first and second collisions.

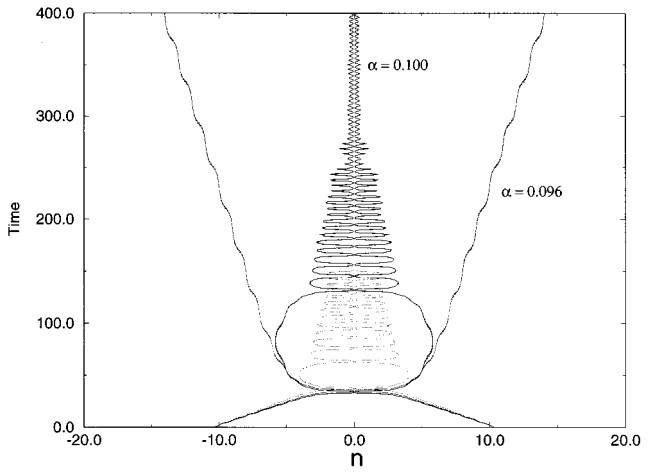

FIG. 5. Trajectories of two colliding localized excitations with different incoming velocities. For $|\alpha|=0.096$, the two localized excitations escape after the first collision. For $|\alpha|=0.100$, the two localized excitations form a breathing bound state upon collision. For comparison, a portion of the trajectory of the bound state for $|\alpha|=0.090$ (dotted line) is also shown. $\beta=1$ and $x_0=10.5$ for the initial profiles (8) and $\mu=1$ and $\nu=-0.1$ in system (1) for all cases.

tions have small kinetic energies. During the collision, these two localized excitations may lose a sufficiently large amount of energy through radiation and they are no longer able to separate because their kinetic energy can no longer overcome the binding energy. This is indeed the case, as we observed in our simulations. However, if there simply existed a velocity threshold below which a bound state is formed and above which two localized excitations escape from each other after the collision, the dynamics would be rather conventional. What we found in the simulations presents a far more intricate picture. First, we show an example of a bound state in Fig. 4 in which two localized excitations collide and then bounce, separating from each other. However, the interaction between the not-too-well separated localized excitations attracts them back to execute a second collision. During this process, they continuously emit small-amplitude radiations. Finally, they can no longer be widely separated. Instead, they merge into a single breathing bound state with a shape that changes from a two-peaked state to a singly peaked state and vice versa, as seen in the last part of the trajectory in Fig. 4. In Fig. 5 we show an example of the advertised resonance phenomenon, that is, the formation of states of one of the above types interlaced between the other type as a function of the incoming velocity. For $\alpha=-0.090$ for the localized excitation on the right-hand side of the figure, the dotted trajectory shows a bound state. By increasing the incoming velocity, e.g., to $\alpha=-0.096$, these two localized excitations begin to separate permanently instead of forming a bound state after the first collision. However, upon further increasing the incoming velocity, say, to $\alpha=-0.100$, a breathing bound state is again formed out of the collision. In Fig. 6 we display the result of our comprehensive numerical search for this kind of resonant structure. In the simulations, the parameter $|\alpha|$ was swept from $|\alpha|=0.0156$ upward, corresponding to increasing incoming velocities starting from $V_{\text{in}}=0.022\,55$. The increment of α was 5×10^{-5}. For incoming velocities below the critical value $V_{\text{in},c}=0.1837$ (above which we only have separating localized excitations, as mentioned above), we have found only one escape velocity window sandwiched between the trapping regions, as shown by the solid line in Fig. 6. Figure 6 plots two quantities as functions of the incoming velocity. One is the escape velocity of the localized excitations (solid line) and the other is Δt, the time between the first and the second collision (see Fig. 4) for the trapped localized excitations in the trapping region of the incoming velocity; here the y coordinate of the upper edge of the shaded area is Δt scaled by a factor of 1000. In those trapping regions, the time interval between the

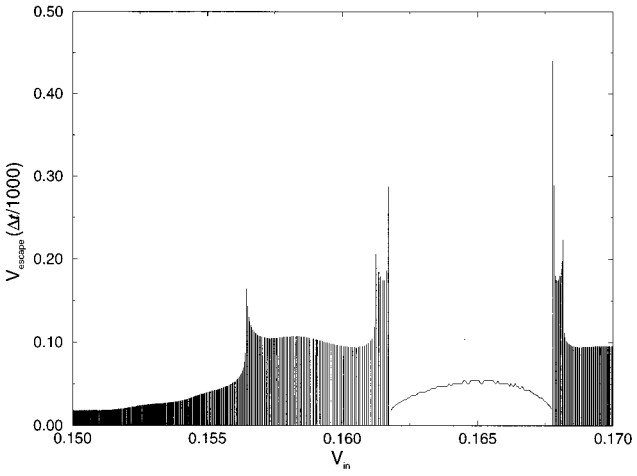

FIG. 6. Escape window in the trapping region. Here two quantities V_{escape} and Δt, as functions of the incoming velocity, are plotted. The solid line is the escape velocity of a localized excitation in the escape region of the incoming velocity. The x coordinate of the shaded area is the incoming velocity for the localized excitations trapped to form a breathing bound state. The y coordinate of the upper edge of the shaded area is the time Δt between the first and second collisions scaled by a factor of 1000 (see Fig. 4). Here $\beta=1$ and $x_0=10.5$ for the initial profile (8); $\mu=1$ and $\nu=-0.1$ in system (1).

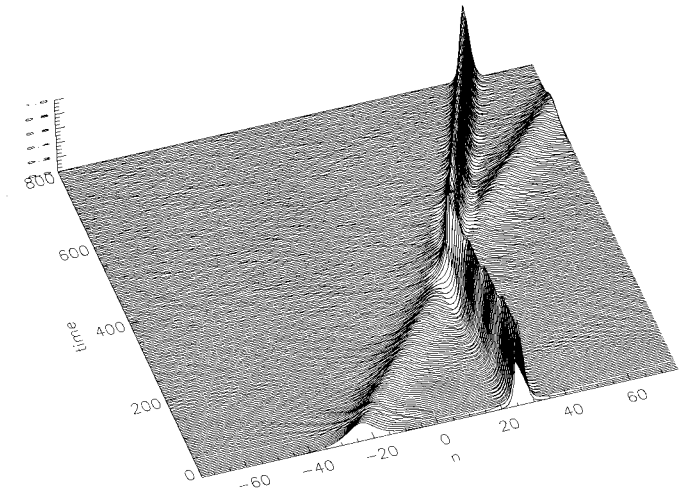

FIG. 7. Case of two localized excitations with different amplitudes passing through each other after the collision. For the large-amplitude excitation $\alpha_1=0$ and $\beta_1=1$; for the low-amplitude excitation, $\alpha_2=0.071\,003$ and $\beta_2=0.25$ for the initial profiles (8), respectively. The system parameters are $\mu=1$ and $\nu=-0.1$. Periodic boundary conditions are used with a total lattice size $N=200$.

first and the second collisions exhibits complex spiked structures. One might suspect that those peaks can be resolved into further escape windows and trapping regions. We have searched those peak regions with α increments of 10^{-7} and have not detected any further escape windows. The small increment of this magnitude has already reached our numerical limits and no further conclusion can be drawn about the existence of those windows smaller than this increment size.

We point out that the above resonance phenomenon is not restricted to equal amplitude localized excitation collisions. In Figs. 7 and 8 two localized excitations with different amplitudes collide and eventually pass through each other. We can clearly see that their asymptotic velocities before and

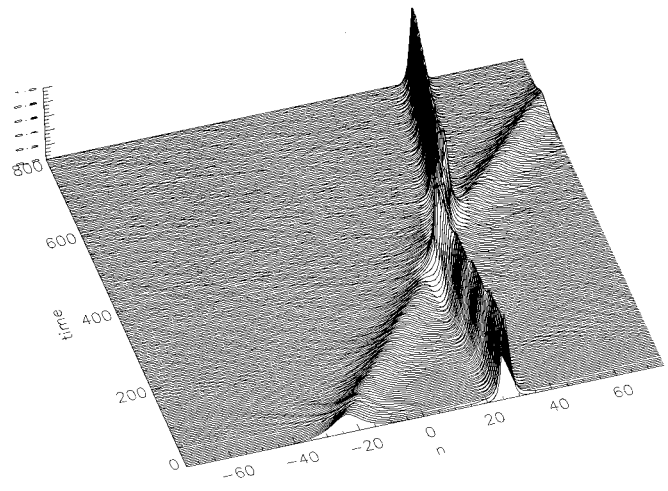

FIG. 8. Case of two localized excitations with different amplitudes passing through each other after the collision. For the large-amplitude excitation, $\alpha_1=0$ and $\beta_1=1$; for the low-amplitude excitation, $\alpha_2=0.070\,975$ and $\beta_2=0.25$. The system parameters are $\mu=1$ and $\nu=-0.1$. Periodic boundary conditions are used with a total lattice size $N=200$.

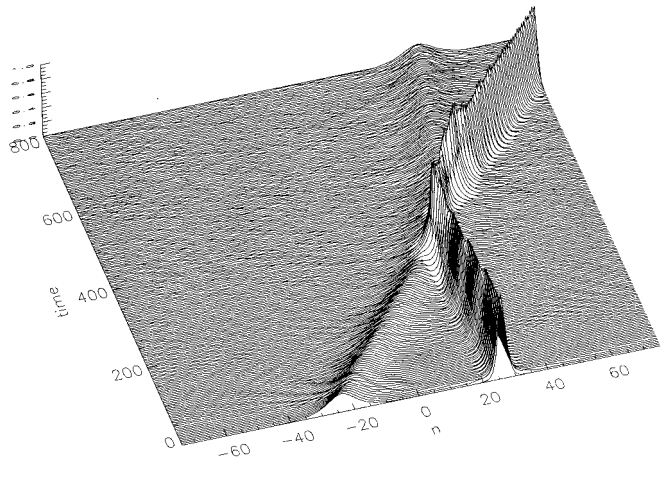

FIG. 9. Collision of two localized excitations with different amplitudes, bouncing off each other after the collision. For the excitation with the large amplitude, $\alpha=0$ and $\beta=1$; for the excitation with the low amplitude, $\alpha_2=0.071\,000$ and $\beta_2=0.25$ for the initial profile (8), respectively. The system parameters are $\mu=1$ and $\nu=-0.1$. Periodic boundary conditions are used with $N=200$.

after the collision are different, depending on the incoming velocities. The localized excitation with the larger amplitude initially is at rest. After the collision, it acquires kinetic energy and starts to translate, unlike in the integrable case in which a soliton initially at rest will not be able to move at a nonzero velocity after collision. In Fig. 9 the localized excitation with the smaller amplitude has an incoming velocity between those of the localized excitations in Figs. 7 and 8. Instead of passing through the large-amplitude localized excitation after the collision, it cannot penetrate and eventually bounces off the large localized excitation. From preliminary numerical results, we have not found any trapping case, i.e., two localized excitations traveling together at the same velocity to form a long-lived bound state after the collision. There are numerical indications that such trapping states may exist but are probably very unstable, i.e., the binding energy is likely to be too small to sustain a long-lived bound state. Although we have not performed an extensive search in the case of two localized excitations with unequal amplitudes, the above examples already illustrate the rich complexity of this collision dynamics.

To complement the collision of two localized excitations with varying incoming velocities, we can alternatively fix α and β for the initial localized excitations and tune the nonintegrable parameter ν in Eq. (1). For the collision of two equal-amplitude localized excitations, we have again found resonance phenomenon in the ν axis as shown in Fig. 10, for which we used an increment of 10^{-4} in ν in our search. For $\nu>0$, it appears that the resonance structure is relatively simple: There exists a threshold in ν above which there are only bound states and below which the two solitons escape from the collision region. For $\nu<0$, there are trapping and escape windows interlacing with each other. For the escape velocity as a function of ν, we also observe a self-similar pattern. We note that there is no new type of states observed, only the bound states and the escaping states discussed previously.

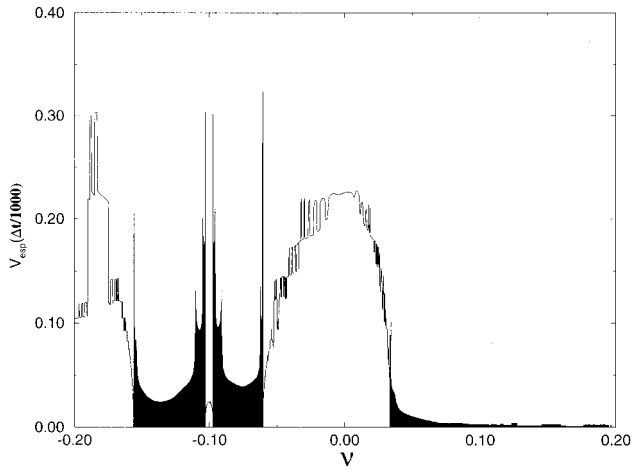

FIG. 10. Resonance structure. Two quantities V_{escape} and Δt are plotted here as functions of ν. The solid line is the escape velocity of a localized excitation after collision in the escape region of ν. The x coordinate in the shaded area is the ν for which two localized excitations are trapped to form a breathing bound state in system (1). The y coordinate of the upper edge of the shaded area is Δt scaled by a factor of 1000 (see Fig. 4). Here $\beta=1$ and $|\alpha|=0.096$ for the initial profile (8).

We emphasize that, for both cases, i.e., varying α and ν, we have not detected any escapes after the second collision. This observation, combined with the fact that all the escapes in the escape window in Fig. 6 are characterized by escape immediately following the first collision, suggests that the mechanism for our resonance structure is different from that of the kink-antikink collision in, e.g., the continuous ϕ^4 system or the modified double sine-Gordon systems [35–37]. There, the delicate timing in the energy exchange between the translational mode and the internal shape mode of a kink (or an antikink) is responsible for the resonant velocity windows. As a consequence, it is necessary for the kink and antikink in the resonant region to collide at least twice before they can escape from each other and separate indefinitely. This is also true of the case in which a kink interacts with a point impurity and the resonating interaction is signified by two consecutive collisions before the kink can escape [38,39]. In the present case, it appears that the energy exchange is subtler, involving the translational energy and the shape modes of the fully formed bound state instead of the shape modes of the individual incoming localized excitations. The nature of these bound states is being investigated currently and will be reported on later.

In conclusion, we have numerically studied the collision dynamics of two solitonlike, localized excitations in the discrete nonlinear Schrödinger chain, system (1). Our simulations have revealed a different resonance phenomenon of interlacing regions of bound states and escaping final states of two localized excitations with a sensitive dependence on the incoming velocities. Our results indicate that the resonance phenomenon in this system might be different from that of the kink-antikink collisions previously studied in ϕ^4 and related systems. We emphasized that the resonance in the system (1) is a combined effect of discreteness and nonintegrability.

[1] For example, Physica D **66** (1 & 2) (1993), special issue on nonlinearity in materials science, edited by A. R. Bishop, R. Ecke, and J. Gubernatis.
[2] For example, Physica D **68** (1) (1993), special issue on future directions of nonlinear dynamics in physical and biological systems, edited by P. L. Christiansen, J. C. Eilbeck, and R. D. Parmentier.
[3] M. J. Ablowitz and P. A. Clarkson, *Solitons, Nonlinear Evolution Equations and Inverse Scattering* (Cambridge University Press, New York, 1991).
[4] L. D. Faddeev and L. A. Takhtajan, *Hamiltonian Methods in the Theory of Solitons* (Springer-Verlag, Berlin, 1987).
[5] Yu. S. Kivshar and B. A. Malomed, Rev. Mod. Phys. **61**, 763 (1989).
[6] S. Flach and C. R. Willis (unpublished).
[7] A. M. Kosevich and A. S. Kovalev, Sov. Phys. JETP **67**, 1793 (1974).
[8] A. J. Sievers and S. Takeno, Phys. Rev. Lett. **61**, 970 (1988).
[9] D. Cai, A. R. Bishop, and N. Grønbech-Jensen, Phys. Rev. Lett. **72**, 591 (1994).
[10] R. S. MacKay and S. Aubry, Nonlinearity **7**, 1623 (1994).
[11] P. C. Bressloff, Phys. Rev. Lett. **75**, 962 (1995).
[12] D. Bambusi, Nonlinearity **9**, 433 (1996).
[13] S. Takeno, J. Phys. Soc. Jpn. **61**, 2821 (1992), and references therein.
[14] D. K. Campbell and M. Peyrard, in *Chaos—Soviet American Perspectives on Nonlinear Science*, edited by D. K. Campbell (American Institute of Physics, New York, 1990).
[15] J. L. Marin and S. Aubry, Nonlinearity **9**, 1501 (1996).
[16] S. Flach, Phys. Rev. E **51**, 1503 (1995).
[17] J. B. Page, Phys. Rev. B **41**, 7835 (1990).
[18] K. W. Sandusky, J. B. Page, and K. E. Schmidt, Phys. Rev. B **46**, 6161 (1992).
[19] V. M. Burlakov, S. A. Kiselev, and V. N. Pyrkov, Solid State Commun. **74**, 327 (1990).
[20] V. M. Burlakov, S. A. Kiselev, and V. N. Pyrkov, Phys. Rev. B **42**, 4921 (1990).
[21] V. M. Burlakov, S. A. Kiselev, and V. I. Pupasov, Phys. Lett. A **147**, 130 (1990).
[22] V. M. Burlakov and S. A. Kiselev, Sov. Phys. JETP **72**, 854 (1991).
[23] R. Bourbonnais and R. Maynard, Phys. Rev. Lett. **64**, 1397 (1990).
[24] S. R. Bickham and A. J. Sievers, Phys. Rev. B **43**, 2339 (1991).
[25] S. R. Bickham, A. J. Sievers, and S. Takeno, Phys. Rev. B **45**, 10 344 (1992).
[26] S. Takeno and K. Hori, J. Phys. Soc. Jpn. **60**, 947 (1990).
[27] T. Dauxois, M. Peyrard, and C. R. Willis, Phys. Rev. E **48**, 4768 (1993).
[28] T. Dauxois and M. Peyrard, Phys. Rev. Lett. **70**, 3935 (1993).
[29] M. Salerno, Phys. Rev. A **46**, 6846 (1992).

[30] D. Cai, A. R. Bishop, and N. Grønbech-Jensen, Phys. Rev. E **53**, 4131 (1996).
[31] D. Henning, N. G. Sun, H. Gabriel, and G. P. Tsironis, Phys. Rev. E **52**, 255 (1995).
[32] D. Hennig, K. Ø. Rasmussen, H. Gabriel, and A. Bülow, Phys. Rev. E **54**, 5788 (1996).
[33] K. Ø. Rasmussen, D. Cai, A. R. Bishop, and N. Grønbech-Jensen, Phys. Rev. E **55**, 6151 (1997).
[34] The equation for the σ time evolution is rather lengthy and we do not reproduce it here.
[35] D. K. Campbell, J. F. Schonfeld, and C. A. Wingate, Physica D **9**, 1 (1983).
[36] M. Peyrard and D. K. Campbell, Physica D **9**, 33 (1983).
[37] D. K. Campbell, M. Peyrard, and P. Sodano, Physica D **19**, 165 (1986).
[38] Yu. S. Kivshar, Z. Fei, and L. Vázquez, Phys. Rev. Lett. **67**, 1177 (1991).
[39] Z. Fei, Yu. S. Kivshar, and L. Vázquez, Phys. Rev. A **45**, 6019 (1992).